

Hyperbolic metamaterial lens with hydrodynamic nonlocal response

Wei Yan, N. Asger Mortensen, and Martijn Wubs*

*Department of Photonics Engineering & Center for Nanostructured Graphene (CNG),
Technical University of Denmark, DK-2800 Kongens Lyngby, Denmark*

[*mwubs@fotonik.dtu.dk](mailto:mwubs@fotonik.dtu.dk)

Abstract: We investigate the effects of hydrodynamic nonlocal response in hyperbolic metamaterials (HMMs), focusing on the experimentally realizable parameter regime where unit cells are much smaller than an optical wavelength but much larger than the wavelengths of the longitudinal pressure waves of the free-electron plasma in the metal constituents. We derive the nonlocal corrections to the effective material parameters analytically, and illustrate the noticeable nonlocal effects on the dispersion curves numerically. As an application, we find that the focusing characteristics of a HMM lens in the local-response approximation and in the hydrodynamic Drude model can differ considerably. In particular, the optimal frequency for imaging in the nonlocal theory is blueshifted with respect to that in the local theory. Thus, to detect whether nonlocal response is at work in a hyperbolic metamaterial, we propose to measure the near-field distribution of a hyperbolic metamaterial lens.

© 2013 Optical Society of America

OCIS codes: (160.1245) Artificially engineered materials; (260.2065) Effective medium theory; (310.6628) Subwavelength structures, nanostructures.

References and links

1. D. R. Smith and D. Schurig, "Electromagnetic wave propagation in media with indefinite permittivity and permeability tensors," *Phys. Rev. Lett.* **90**, 077405 (2003).
2. I. I. Smolyaninov, "Vacuum in a Strong Magnetic Field as a Hyperbolic Metamaterial," *Phys. Rev. Lett.* **107**, 253903 (2011).
3. H. N. S. Krishnamoorthy, Z. Jacob, E. Narimanov, I. Kretzschmar, and V. M. Menon, "Topological transitions in metamaterials," *Science* **336**, 205–209 (2012).
4. Z. Jacob, I. Smolyaninov, and E. Narimanov, "Broadband Purcell effect: Radiative decay engineering with metamaterials," *Appl. Phys. Lett.* **100**, 181105 (2012).
5. A. N. Poddubny, P. A. Belov, G. V. Naik, and Y. S. Kivshar, "Spontaneous radiation of a finite-size dipole emitter in hyperbolic media," *Phys. Rev. A* **84**, 023807 (2011).
6. T. Tumkur, G. Zhu, P. Black, Y. A. Barnakov, C. E. Bonner, and M. A. Noginov, "Control of spontaneous emission in a volume of functionalized hyperbolic metamaterial," *Appl. Phys. Lett.* **99**, 151115 (2011).
7. M. A. Noginov, Y. A. Barnakov, G. Zhu, T. Tumkur, H. Li, and E. E. Narimanov, "Bulk photonic metamaterial with hyperbolic dispersion," *Appl. Phys. Lett.* **94**, 151105 (2009).
8. P. Belov and Y. Hao, "Subwavelength imaging at optical frequencies using a transmission device formed by a periodic layered metal-dielectric structure operating in the canalization regime," *Phys. Rev. B* **73**, 113110 (2006).
9. B. Wood, J. Pendry, and D. Tsai, "Directed subwavelength imaging using a layered metal-dielectric system," *Phys. Rev. B* **74**, 115116 (2006).
10. X. Li, S. He, and Y. Jin, "Subwavelength focusing with a multilayered Fabry-Perot structure at optical frequencies," *Phys. Rev. B* **75**, 045103 (2007).
11. A. Salandrino and N. Engheta, "Far-field subdiffraction optical microscopy using metamaterial crystals: Theory and simulations," *Phys. Rev. B* **74**, 075103 (2006).

12. Z. Jacob, L. Alekseyev, and E. Narimanov, "Optical hyperlens: Far-field imaging beyond the diffraction limit," *Opt. Express* **14**, 8427–8256 (2006).
13. Z. Liu, H. Lee, Y. Xiong, C. Sun, and X. Zhang, "Far-field optical hyperlens magnifying sub-diffraction-limited objects," *Science* **315**, 1686 (2007).
14. M. Yan and N. A. Mortensen, "Hollow-core infrared fiber incorporating metal-wire metamaterial," *Opt. Express* **17**, 14851–14864 (2009).
15. C. L. Cortes, W. Newman, S. Molesky, and Z. Jacob, "Quantum nanophotonics using hyperbolic metamaterials," *J. Opt.* **14**, 063001 (2012).
16. J. Elser, V. Podolskiy, I. Salakhutdinov, and I. Avrutsky, "Nonlocal effects in effective-medium response of nanolayered metamaterials," *Appl. Phys. Lett.* **90**, 191109 (2007).
17. A. Chebykin, A. Orlov, A. Vozianova, S. Maslovski, Y. S. Kivshar, and P. Belov, "Nonlocal effective medium model for multilayered metal-dielectric metamaterials," *Phys. Rev. B* **84**, 115438 (2011).
18. A. Chebykin, A. Orlov, C. Simovski, Y. S. Kivshar, and P. Belov, "Nonlocal effective parameters of multilayered metal-dielectric metamaterials," *Phys. Rev. B* **86**, 115420 (2012).
19. L. Shen, T. Yang, and Y. Chau, "Effect of internal period on the optical dispersion of indefinite-medium materials," *Phys. Rev. B* **77**, 205124 (2008).
20. L. Shen, T. Yang, and Y. Chau, "50/50 beam splitter using a one-dimensional metal photonic crystal with parabolic-like dispersion," *Appl. Phys. Lett.* **90**, 251909 (2007).
21. F. Bloch, "Bremsvermögen von Atomen mit mehreren Elektronen," *Z. Phys. A* **81**, 363–376 (1933).
22. A. D. Boardman, *Electromagnetic Surface Modes* (John Wiley and Sons, Chichester, 1982).
23. W. L. Mochán, M. Castillo-Mussot, and R. G. Barrera, "Effect of plasma waves on the optical properties of metal-insulator superlattices," *Phys. Rev. B* **15**, 1088–1098 (1987).
24. C. David and F. J. García de Abajo, "Spatial nonlocality in the optical response of metal nanoparticles," *J. Phys. Chem. C* **115**, 19470–19475 (2011).
25. F. J. García de Abajo, "Nonlocal effects in the plasmons of strongly interacting nanoparticles, dimers, and waveguides," *J. Phys. Chem. C* **112**, 17983–17987 (2008).
26. S. Raza, G. Toscano, A.-P. Jauho, M. Wubs, and N. A. Mortensen, "Unusual resonances in nanoplasmonic structures due to nonlocal response," *Phys. Rev. B* **84**, 121412(R) (2011).
27. J. A. Scholl, A. L. Koh, and J. A. Dionne, "Quantum plasmon resonances of individual metallic nanoparticles," *Nature* **483**, 421–427 (2012).
28. C. Ciraci, R. T. Hill, J. J. Mock, Y. Urzhumov, A. I. Fernández-Domínguez, S. A. Maier, J. B. Pendry, A. Chilkoti, and D. R. Smith, "Probing the ultimate limits of plasmonic enhancement," *Science* **337**, 1072–1074 (2012).
29. S. Raza, N. Stenger, S. Kadkhodazadeh, S. V. Fischer, N. Kostesha, A.-P. Jauho, A. Burrows, M. Wubs, and N. A. Mortensen, "Blueshift of the surface plasmon resonance in silver nanoparticles studied with EELS," *Nanophotonics* **2**, 131 (2013).
30. G. Toscano, S. Raza, A.-P. Jauho, M. Wubs, and N. A. Mortensen, "Modified field enhancement and extinction in plasmonic nanowire dimers due to nonlocal response," *Opt. Express* **13**, 4176–4188 (2012).
31. G. Toscano, S. Raza, S. Xiao, M. Wubs, A.-P. Jauho, S. I. Bozhevolnyi, and N. A. Mortensen, "Surface-enhanced Raman spectroscopy (SERS): nonlocal limitations," *Opt. Lett.* **37**, 2538–2540 (2012).
32. A. I. Fernández-Domínguez, A. Wiener, F. J. García-Vidal, S. A. Maier, and J. B. Pendry, "Transformation-optics description of nonlocal effects in plasmonic nanostructures," *Phys. Rev. Lett.* **108**, 106802 (2012).
33. W. Yan, M. Wubs, and N. A. Mortensen, "Hyperbolic metamaterials: nonlocal response regularizes broadband supersingularity," *Phys. Rev. B* **86**, 205429 (2012).
34. P. Jewsbury, "Electrodynamic boundary conditions at metal interfaces," *J. Phys. F: Met. Phys.* **11**, 195–206 (1981).
35. R. C. Monreal, T. J. Antosiewicz, and S. P. Apell, "Plasmons do not go that quantum," arXiv:1304.3023 (2013).
36. L. Stella, P. Zhang, F. J. García-Vidal, A. Rubio, and P. García-González, "Performance of nonlocal optics when applied to plasmonic nanostructures," *J. Phys. Chem. C* **117**, 8941–8949 (2013).
37. T. Teperik, P. Nordlander, J. Aizpurua, and A. G. Borisov, "Quantum plasmonics: Nonlocal effects in coupled nanowire dimer," arXiv:1302.3339 (2013).
38. K. Andersen, K. L. Jensen, and K. S. Thygesen, "Hybridization of quantum plasmon modes in coupled nanowires: From the classical to the tunneling regime," arXiv:1304.4754 (2013).
39. N. Formica, D. S. Ghosh, A. Carrilero, T. L. Chen, R. E. Simpson, and V. Pruneri, "Ultrastable and Atomically Smooth Ultrathin Silver Films Grown on a Copper Seed Layer," *ACS Appl. Mater. Interfaces* **5**, 3048–3053 (2013).

1. Introduction

Hyperbolic metamaterials (HMMs), also known as indefinite media, enjoy a great deal of attention owing to their unique hyperbolic dispersion relations [1–14], with associated high-wavenumber propagating waves without upper limit. This leads to numerous applications, such

as enhanced-light interactions [4–7], subwavelength imaging [8–13], negative refraction [1], and low-loss fiber cladding [14]. HMMs are now also emphasized for their potential applications in quantum nanophotonics [15]. The HMMs are usually artificially made by periodic dielectric-metal structures, such as a 1D dielectric-metal Bragg grating. To describe the optical properties of the HMMs, it is common to employ the local-response approximation (LRA), *i.e.* with every location \mathbf{r} in the structure a certain value for the permittivity $\epsilon(\mathbf{r})$ is associated. In the LRA, the effective material parameters of HMMs have been thoroughly studied [16–20].

Thanks to advances in nanofabrication, we witness a miniaturization of the feature size of metamaterials towards the deep nanoscale. The LRA becomes more inaccurate, since the nonlocal response of free electrons starts to play a role [21–33]. It is known that the nonlocal response causes a blueshift of the surface plasmon (SP) resonance of the metallic particle [26–29], and limits the SP field enhancement that in the LRA sometimes diverges [30–32]. We employ a simple generalization to the LRA, namely the hydrodynamic Drude model (HDM) [21, 22], which takes the nonlocal response into account. New in this model, as compared to the LRA, are longitudinal waves with sub-nanometer wavelengths, besides the usual transverse waves.

Incidentally, some HMMs have been found to exhibit strong effective ‘nonlocal response’, even in studies that employ the local-response approximation [16–20]. What is meant here is that the HMMs, when considered as scatterers, cannot be described in the single-scattering Born approximation. This differs from the (material) nonlocal response of HMMs that we consider here and in Ref. [33], where already the scattering *potentials* associated with the metal constituents are nonlocal.

We recently showed that material nonlocal response plays an important role on HMMs in the limit of vanishing unit-cell size [33]. In particular, the nonlocal response gives rise to a cutoff to the hyperbolic dispersion curve, and an associated finite but very large fundamental upper limit to the enhanced local optical density of states (LDOS), which in the LRA is known to diverge in the limit of vanishingly small unit cells. Now in realized HMMs, it is predominantly the finite size of the unit cell that keeps the LDOS finite. So it is an intriguing question, not explored yet as far as we know, whether nonlocal response can also have noticeable effects in state-of-the-art HMMs. This theoretical paper describes our search for observable nonlocal effects in HMMs with unit cells much smaller than an optical wavelength, but much larger than the wavelength of hydrodynamic longitudinal pressure waves.

2. Dispersion relations of hyperbolic metamaterials

As the HMM we consider a 1D subwavelength dielectric-metal Bragg grating, with a unit cell of thickness d , and thicknesses a and b of the dielectric and metal layers, respectively. The permittivity of the dielectric layer is ϵ_d . The metal is described in the HDM as a free-electron plasma with [21, 22, 26]

$$\epsilon_m^T(\omega) = 1 - \frac{\omega_p^2}{\omega^2 + i\omega\gamma}, \quad \epsilon_m^L(k, \omega) = 1 - \frac{\omega_p^2}{\omega^2 + i\omega\gamma - \beta^2 k^2}, \quad (1)$$

where ϵ_m^T is the Drude permittivity for the transverse electric fields as in the LRA, while the wavevector dependence of the permittivity ϵ_m^L of the longitudinal electric fields is responsible for the nonlocal response.

We apply the hydrodynamic generalization of the common transfer-matrix method for lay-

ered systems [23, 33], and obtain the exact dispersion equation of the HMM

$$\begin{aligned} \cos \theta_b = & \left\{ \cos \theta_d \left[k_{\perp m}^L \cos \theta_m \sin \theta_l - \frac{k_{\parallel} (w_d - w_m)}{z_m} \sin \theta_m \cos \theta_l \right] + \frac{k_{\parallel} (w_d - w_m)}{z_d} \sin \theta_d \right. \\ & \left. (1 - \cos \theta_m \cos \theta_l) - \frac{1}{2} \left[\frac{k_{\parallel}^2}{k_{\perp m}^L} \frac{(w_d - w_m)^2}{z_d z_m} + k_{\perp m}^L \left(\frac{z_d}{z_m} + \frac{z_m}{z_d} \right) \right] \sin \theta_m \sin \theta_l \right\} \\ & \left[k_{\perp m}^L \sin \theta_l - k_{\parallel} \frac{(w_d - w_m)}{z_m} \sin \theta_m \right]^{-1}, \end{aligned} \quad (2)$$

where for convenience we introduced the dimensionless parameters

$$\theta_b = k_{\perp d} d, \quad \theta_d = k_{\perp d} a, \quad \theta_m = k_{\perp m}^T b, \quad \theta_l = k_{\perp m}^L b, \quad (3a)$$

$$z_d = \frac{k_{\perp d}}{k_0 \epsilon_d}, \quad w_d = \frac{k_{\parallel}}{k_0}, \quad z_m = \frac{k_{\perp m}^T}{k_0 \epsilon_m^T}, \quad w_m = \frac{k_{\parallel}}{k_0 \epsilon_m^T}, \quad (3b)$$

and where k_{\perp} represents the Bloch wavevector in the direction of the periodicity, k_{\parallel} the wavevector along the layers, and $k_0 = \omega/c$ the free-space wavevector. We also introduced the derived wavevectors $k_{\perp d} = \sqrt{k_0^2 \epsilon_d - k_{\parallel}^2}$, $k_{\perp m}^T = \sqrt{k_0^2 \epsilon_m^T - k_{\parallel}^2}$, and $k_{\perp m}^L = \sqrt{(\omega^2 + i\gamma\omega - \omega_p^2)/\beta^2 - k_{\parallel}^2}$.

We note that solving the hydrodynamic Drude model requires boundary conditions in addition to the usual Maxwell boundary conditions. The dispersion relation Eq. (2) was derived using the continuity of the normal component of the free-electron current as the additional boundary condition. Details can be found in Refs. [26, 33, 34]. The exact dispersion relation for nonlocal response Eq. (2) reduces to the exact dispersion relation in the LRA by putting the longitudinal permittivity $\epsilon_m^L(k, \omega)$ of Eq. (1) equal to the transverse permittivity $\epsilon_m^T(\omega)$ of Eq. (1), in other words by taking the nonlocal parameter β to zero.

3. Effective nonlocal material parameters

As stated before, we consider sub-wavelength unit cells much smaller than optical wavelengths, but with metal layers much larger than the wavelengths of their longitudinal pressure waves. So we focus on the situation where the following two parameters are small,

$$k_0 d \ll 1, \quad \frac{1}{|k_{\perp m}^L b|} \ll 1, \quad (4)$$

where $k_{\perp m}^L = \sqrt{\omega^2 + i\gamma\omega - \omega_p^2}/\beta$ is the longitudinal wavevector. Furthermore, we will only consider the frequency range $\omega < \omega_p$, where $\epsilon_m^T < 0$ and the dispersion curve of the HMM could be a hyperbola in the LRA. We now make a first-order Taylor approximation in the small parameters of Eq. (4) to the exact dispersion relation Eq. (2), and obtain the approximate dispersion relation

$$k_{\perp}^2 = k_0^2 \epsilon_{\parallel}^{\text{loc}} - k_{\parallel}^2 \frac{\epsilon_{\parallel}^{\text{loc}}}{\epsilon_{\perp}^{\text{loc}}} - \left\{ k_{\parallel}^2 \frac{\epsilon_{\parallel}^{\text{loc}}}{\epsilon_{\perp}^{\text{hd}}} + \Delta_{\text{la}} \right\}. \quad (5)$$

The two terms in the brace are two leading correction terms that originate from the nonlocal response of the free electrons and from the finite size of the unit cell, respectively. Without them, *i.e.* when neglecting both the finiteness of the unit cells and nonlocal response, we have the well-known dispersion relation in the LRA

$$k_{\perp}^2 = k_0^2 \epsilon_{\parallel}^{\text{loc}} - k_{\parallel}^2 \frac{\epsilon_{\parallel}^{\text{loc}}}{\epsilon_{\perp}^{\text{loc}}}, \quad (6)$$

where $\epsilon_{\parallel}^{\text{loc}}$ and $\epsilon_{\perp}^{\text{loc}}$ are the effective local permittivities [9]

$$\epsilon_{\parallel}^{\text{loc}} = f_d \epsilon_d + f_m \epsilon_m, \quad \epsilon_{\perp}^{\text{loc}} = \frac{1}{f_d \epsilon_d^{-1} + f_m \epsilon_m^{-1}}, \quad (7)$$

where $f_d = a/d$ and $f_m = b/d$. We note that Eq. (7) is satisfied when the unit-cell thickness is much smaller than the free-space wavelength indicated by the first inequality in Eq. (4). Obviously, when $\epsilon_{\parallel}^{\text{loc}} \epsilon_{\perp}^{\text{loc}} < 0$, Eq. (6) describes a hyperbolic dispersion curve. However, we are now rather interested in nonlocal response effects in realistic HMMs, so we investigate the importance of the terms in the brace in Eq. (5), which are given in terms of

$$\epsilon_{\perp}^{\text{hdm}} = \frac{k_m^L d}{2i} \frac{\epsilon_m^T}{\epsilon_m^T - 1} \quad \text{and} \quad (8a)$$

$$\begin{aligned} \Delta_{\text{la}} = & \frac{1}{12} \epsilon_d \epsilon_m^T f_d f_m d^2 \left(k_0^2 - \frac{k_{\parallel}^2}{\epsilon_{\perp}^{\text{loc}}} \right)^2 \\ & + \frac{1}{12} \epsilon_{\parallel}^{\text{loc}} d^2 \left[2k_{\perp d}^2 (k_{\perp m}^T)^2 f_m f_d \frac{\epsilon_{\parallel}^{\text{loc}}}{\epsilon_d \epsilon_m^T} + (k_{\perp d})^4 \frac{f_d^3}{\epsilon_d} + k_{\perp m}^T{}^4 \frac{f_m^3}{\epsilon_m^T} \right]. \end{aligned} \quad (8b)$$

From the expression (8a) for $\epsilon_{\perp}^{\text{hdm}}$, it follows that the local-response limit is found in the limit $k_m^L d \rightarrow \infty$ rather than by taking the size d of the unit cell to zero, see also Ref. [33] on this point. In the following we will keep the first (*i.e.* the nonlocal) correction term, while neglecting the other correction term Δ_{la} . The sole justification for doing so is that the second term turns out to be negligible in comparison to the first one for the HMMs that we consider, as we illustrate numerically below. So, as an improved approximation to Eq. (6), we keep the correction term concerning $\epsilon_{\perp}^{\text{hdm}}$, and then obtain the approximate nonlocal dispersion relation that is central to our present study,

$$k_{\perp}^2 = k_0^2 \epsilon_{\parallel}^{\text{loc}} - k_{\parallel}^2 \frac{\epsilon_{\parallel}^{\text{loc}}}{\epsilon_{\perp}^{\text{nloc}}}, \quad (9)$$

in terms of the new effective permittivity in the direction of the periodicity corrected by the nonlocal response

$$\frac{1}{\epsilon_{\perp}^{\text{nloc}}} = \frac{1}{\epsilon_{\perp}^{\text{loc}}} + \frac{1}{\epsilon_{\perp}^{\text{hdm}}}. \quad (10)$$

The other tensor component $\epsilon_{\parallel}^{\text{loc}}$ of the dielectric tensor has no such nonlocal correction.

Since $1/|k_m^L d| \ll 1$, we usually have $\epsilon_{\perp}^{\text{loc}} \ll \epsilon_{\perp}^{\text{hdm}}$, and then $\epsilon_{\perp}^{\text{nloc}} \approx \epsilon_{\perp}^{\text{loc}}$ is a good approximation. However, for large $\epsilon_{\perp}^{\text{loc}}$ and especially in the extreme case that $\epsilon_{\perp}^{\text{loc}} \rightarrow \infty$, it may occur that $\epsilon_{\perp}^{\text{loc}}$ becomes much larger than $\epsilon_{\perp}^{\text{hdm}}$, so that $\epsilon_{\perp}^{\text{nloc}} \approx \epsilon_{\perp}^{\text{hdm}}$ by virtue of Eq. (10). So in this case, the nonlocal response has the important role of replacing the infinite $\epsilon_{\perp}^{\text{loc}}$ by the finite $\epsilon_{\perp}^{\text{hdm}}$ in the dispersion relation. But when does it occur that $\epsilon_{\perp}^{\text{loc}} \rightarrow \infty$? This immediately follows from Eq. (7), and occurs when $f_d \epsilon_d^T + f_m \epsilon_d$ vanishes. In particular, neglecting the Drude damping γ of the metal, the frequency $\omega_{\text{res}}^{\text{loc}}$ for which $\epsilon_{\perp}^{\text{loc}} \rightarrow \infty$ is given by

$$\omega_{\text{res}}^{\text{loc}} = \omega_p \sqrt{\frac{f_d}{f_d + f_m \epsilon_d}}. \quad (11)$$

Let us also consider another extreme case, namely $\epsilon_{\perp}^{\text{nloc}} \rightarrow \infty$. This is achieved when $\epsilon_{\perp}^{\text{loc}} = -\epsilon_{\perp}^{\text{hdm}}$, which happens at the frequency

$$\omega_{\text{res}}^{\text{nloc}} \approx \omega_{\text{res}}^{\text{loc}} \left(1 + \frac{\epsilon_d}{k_m^L a} \right). \quad (12)$$

At this frequency $\omega_{\text{res}}^{\text{nlloc}}$, the nonlocal response changes the finite $\epsilon_{\perp}^{\text{loc}}$ into the infinite $\epsilon_{\perp}^{\text{nlloc}}$, again a strong nonlocal effect.

From the above analysis, it follows that nonlocal response is important for HMMs near the frequencies $\omega_{\text{res}}^{\text{loc}}$ and $\omega_{\text{res}}^{\text{nlloc}}$, as also evidenced numerically in the next section. The larger the difference between $\omega_{\text{res}}^{\text{loc}}$ and $\omega_{\text{res}}^{\text{nlloc}}$, the broader the frequency range with noticeable nonlocal effects. As indicated by Eqs. (11) and (12), the nonlocal resonance frequency $\omega_{\text{res}}^{\text{nlloc}}$ is blueshifted with respect to the local one $\omega_{\text{res}}^{\text{loc}}$. The relative blueshift $(\omega_{\text{res}}^{\text{nlloc}} - \omega_{\text{res}}^{\text{loc}})/\omega_{\text{res}}^{\text{loc}}$ is proportional to ϵ_d , and inversely proportional to the dimensionless parameter $k_m^L a$. The latter dependence is rather surprising, since k_m^L is the longitudinal wavevector of the free electrons in the metal layers, whereas a is the thickness of the dielectric layer! We checked, also numerically, that our first-order Taylor expansion of the dispersion relation in the small parameter $(k_m^L b)^{-1}$ indeed gives a relative blueshift $\epsilon_d/(k_m^L a)$, independent of the thickness b of the metal layer.

To give a physical explanation on nonlocal blue-shift independent of the metal layer thickness, we simplify the discussion by considering the dielectric layer being free space with $\epsilon_d = 1$. From Eq. (11), we have the local resonance frequency $\omega_{\text{res}}^{\text{loc}} = \omega_p \sqrt{a/d}$. With nonlocal response, the surface charge at the metal boundary is smeared out. Effectively, we could view the surface charge as being displaced into the metal layer by a distance of $1/k_m^L$. Accordingly, the effective thickness of the free-space layer is increased to $a_{\text{eff}} = a + 2/k_m^L$, where the factor 2 comes from the two interface boundaries of the metal layer. Taking a_{eff} into Eq. (11), we have $\omega_{\text{res}}^{\text{nlloc}} \approx \omega_{\text{res}}^{\text{loc}}(1 + 1/(k_m^L a))$, which is just Eq. (12) with $\epsilon_d = 1$, and independent of the metal layer thickness.

4. Effects of nonlocal response on the dispersion curve: numerical analysis

To numerically illustrate the effects of the nonlocal response on the HMM, we choose a specific example of the HMM with $a = 6\text{nm}$, $b = 3\text{nm}$, and $\epsilon_d = 10$. We choose the metal to be Au, and describe it by only its free-electron response, with parameters $\hbar\omega_p = 8.812\text{eV}$, $\hbar\gamma = 0.0752\text{eV}$, and $v_F = 1.39 \times 10^6\text{m/s}$. Here, we note that it is a tough task to fabricate the HMM with a unit cell of a 3nm-thick metal layer and a dielectric layer of 6nm. However, with further progress in nano-fabrication techniques, we believe that such a HMM structure will be practically feasible in the near future. For example, very recently experimentalists have succeeded in fabricating a 3nm-thick Ag film by depositing the film on a 1nm copper seed layer [39].

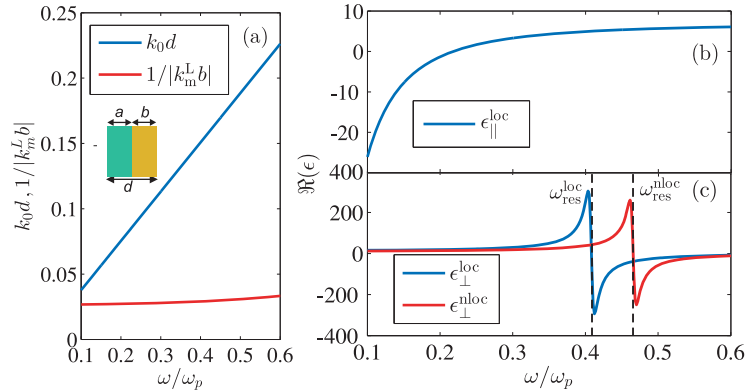


Fig. 1. (a) $k_0 d$ and $1/|k_m^L b|$, (b) real part of $\epsilon_{\parallel}^{\text{loc}}$, and (c) real parts of $\epsilon_{\perp}^{\text{loc}}$ and $\epsilon_{\perp}^{\text{nlloc}}$, of the HMM. The unit cell of the HMM shown in the inset of (a) has $a = 6\text{nm}$, $b = 3\text{nm}$, $\epsilon_d = 10$, and the yellow metal layer is Au.

Figure 1(a) shows the value of k_0d and $1/|k_m^L b|$. Clearly, in the frequency range $0.1\omega_p < \omega < 0.6\omega_p$, both k_0d and $1/|k_m^L b|$ satisfy Eq. (4). This indicates that we are in the regime where the analytical results of the above section are valid. Figure 1(b) displays the real part of $\epsilon_{\parallel}^{\text{loc}} = \epsilon_{\parallel}^{\text{nlloc}}$, and Fig. 1(c) the real parts $\epsilon_{\perp}^{\text{loc}}$ and $\epsilon_{\perp}^{\text{nlloc}}$. The two dashed vertical lines in Fig. 1(c) mark the positions of $\omega_{\text{res}}^{\text{loc}}$ and $\omega_{\text{res}}^{\text{nlloc}}$ as calculated with the approximate but accurate Eqs. (11) and (12), respectively. With the damping loss of the metal, $\epsilon_{\perp}^{\text{loc}}$ and $\epsilon_{\perp}^{\text{nlloc}}$ show large but finite values near $\omega_{\text{res}}^{\text{loc}}$ and $\omega_{\text{res}}^{\text{nlloc}}$, respectively. Around $\omega_{\text{res}}^{\text{loc}}$ and $\omega_{\text{res}}^{\text{nlloc}}$, $\epsilon_{\perp}^{\text{loc}}$ and $\epsilon_{\perp}^{\text{nlloc}}$ show a huge difference, indicating the importance of nonlocal response, consistent with the theoretical prediction in the previous section. Far from $\omega_{\text{res}}^{\text{loc}}$ and $\omega_{\text{res}}^{\text{nlloc}}$, the dielectric functions $\epsilon_{\perp}^{\text{loc}}$ and $\epsilon_{\perp}^{\text{nlloc}}$ are nearly equal, so that away from these resonances the nonlocal response is only a small perturbation.

Figure 2(a) and (b) illustrate the dispersion curves at $\omega = 0.1\omega_p$ and $\omega = 0.6\omega_p$, respectively. These frequencies are far away from the resonances $\omega_{\text{res}}^{\text{loc}}$ and $\omega_{\text{res}}^{\text{nlloc}}$. The small damping loss is neglected for a clearer illustration of the dispersion curve. Several observations can be extracted from Fig. 2. Firstly, the exact local and nonlocal dispersion curves agree well with those based on the effective material parameters, which confirms the validity of the approximate theoretical results of Sec. 3. Secondly, the local and nonlocal curves only show a slight difference, agreeing well with Fig. 1(c) where we see $\epsilon_{\perp}^{\text{nlloc}} \approx \epsilon_{\perp}^{\text{loc}}$ both for $\omega = 0.1\omega_p$ and $0.6\omega_p$.

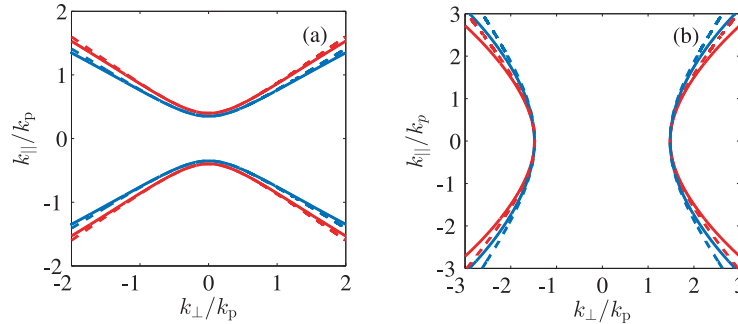


Fig. 2. Dispersion curves of the HMM at (a) $\omega = 0.1\omega_p$ and (b) $\omega = 0.6\omega_p$. The HMM is as that in Fig. 1 except that the loss is neglected. Red solid curves for the exact local dispersion, blue solid curves for the exact nonlocal dispersion, red dashed curves for the approximated local dispersion of Eq. (6), and blue dashed curves for the approximated nonlocal dispersion of Eq. (9).

Figure 3(a) and (b) show the on-resonance dispersion curves, namely for $\omega = \omega_{\text{res}}^{\text{loc}} = 0.41\omega_p$ and for $\omega = \omega_{\text{res}}^{\text{nlloc}} = 0.465\omega_p$, respectively. Loss is again neglected, as in Fig. 2. At both frequencies, the nonlocal response modifies the dispersion curve noticeably. In particular, at $\omega = 0.41\omega_p$, the local dispersion curve consists of two nearly flat lines of $k_{\perp} = \pm k_0 \sqrt{\epsilon_{\parallel}^{\text{loc}}}$. With the nonlocal response, however, the dispersion curve becomes a closed ellipse! This remarkable difference can be understood from the difference between $\epsilon_{\perp}^{\text{loc}}$ and $\epsilon_{\perp}^{\text{nlloc}}$. In particular, $\epsilon_{\perp}^{\text{loc}}$ diverges while $\epsilon_{\perp}^{\text{nlloc}} = 41$ stays finite in the lossless case. When including the loss, the effective parameters change to $\epsilon_{\perp}^{\text{loc}} = -200 + 500i$ and $\epsilon_{\perp}^{\text{nlloc}} = 43.7 + 3i$. The loss would only slightly modify the dispersion curves of Fig. 3(a). In Fig. 3(b) we display dispersion relations at $\omega = 0.465\omega_p$. Here the local dispersion curve is a hyperbola. With the nonlocal response, however, the dispersion curve becomes nearly flat lines, which can be attributed to the extremely large value of $\epsilon_{\perp}^{\text{nlloc}}$ at this frequency $\omega_{\text{res}}^{\text{nlloc}}$.

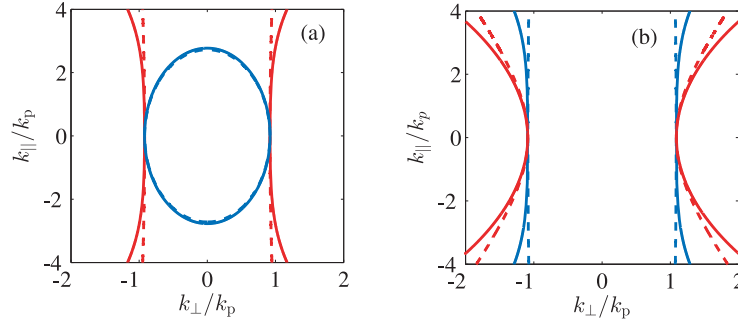


Fig. 3. Dispersion curves of the HMM at (a) $\omega = \omega_{\text{res}}^{\text{loc}} = 0.41\omega_p$ and (b) $\omega = \omega_{\text{res}}^{\text{nlc}} = 0.465\omega_p$. The HMM is as that in Fig. 1 except that the loss is neglected. Red solid curves denote the exact local dispersion, blue solid curves the exact nonlocal dispersion; red dashed curves for the approximated local dispersion curves of Eq. (6), and blue dashed curves for the approximated dispersion curves of Eq. (9).

5. Effects of nonlocal response on a hyperbolic metamaterial lens

A HMM slab can operate as a superlens with subwavelength resolution, since the hyperbolic dispersion curve supports propagating waves with arbitrarily high wavevectors, which can transfer the evanescent information of the object. In the LRA, it is known that the HMM with its flat dispersion curve at $\omega_{\text{res}}^{\text{loc}}$ [recall Fig. 3(a)] is especially favorable for subwavelength imaging [8, 12]. The reason is that the flat dispersion curve with the constant k_{\perp} ensures that all plane-wave components experience the same phase changes after transmission through the HMM slab, at least if reflections can be neglected. Actually, the reflections can be suppressed by appropriate choice of the thickness l of the HMM lens, and even be made to vanish by choosing $k_{\perp}l = n\pi$, where n is a positive integer. In theory this could lead to a perfect image at $x = 0$.

Let us now investigate how nonlocal response may influence the subwavelength imaging characteristics of the HMM lens. As demonstrated in the above sections, the nonlocal response sets the infinite $\epsilon_{\perp}^{\text{loc}} \rightarrow \infty$ to a finite value and accordingly destroys the desired flat dispersion curve at the frequency $\omega_{\text{res}}^{\text{loc}}$ where one would normally choose to operate for perfect imaging, based on the LRA. Nevertheless, at a blueshifted frequency $\omega_{\text{res}}^{\text{nlc}}$, the local effective dielectric function $\epsilon_{\perp}^{\text{loc}}$ may be finite, but the hydrodynamic Drude model predicts instead that $\epsilon_{\perp}^{\text{nlc}}$ diverges, with the concomitant flat dispersion curve suitable for subwavelength imaging. Thus nonlocal response is expected to strongly affect the performance of HMM superlenses for frequencies ω around $\omega_{\text{res}}^{\text{loc}}$ and $\omega_{\text{res}}^{\text{nlc}}$.

As an example, we consider a HMM slab with $l = 36d$, *i.e.* composed of 36 unit cells, in a free-space background with the two boundaries at $x = -l$ and $x = 0$. The unit cell is as in Fig. 1, and is arranged in a symmetric sandwich structure with the metal layer at the center. A line dipole source is positioned to the left of the HMM slab, with x -coordinate $-l - x_s$ and y -coordinate 0, and is represented by $\mathbf{J} = \delta(x + l + x_s)\delta(y)\hat{y}$. We choose the distance to the HMM slab to be $x_s = 10\text{nm}$. The interaction between the current source and the HMM slab is solved by using the transfer-matrix method of Refs. [23, 33].

Figure 4(a) and (b) demonstrate the transmitted electric-field intensity at $\omega = \omega_{\text{res}}^{\text{loc}} = 0.41\omega_p$ for local and nonlocal response, respectively. Metal loss is taken into account. The spatial coordinates in Fig. 4(a) and (b) are normalized by the free-space wavelength λ_p that corresponds to the plasma frequency. In the local case, we have the known the dispersion of Fig. 3(a) featuring flat lines. There $k_{\perp}l$ approximately equals $\approx 4.25\pi$, indicating that reflec-

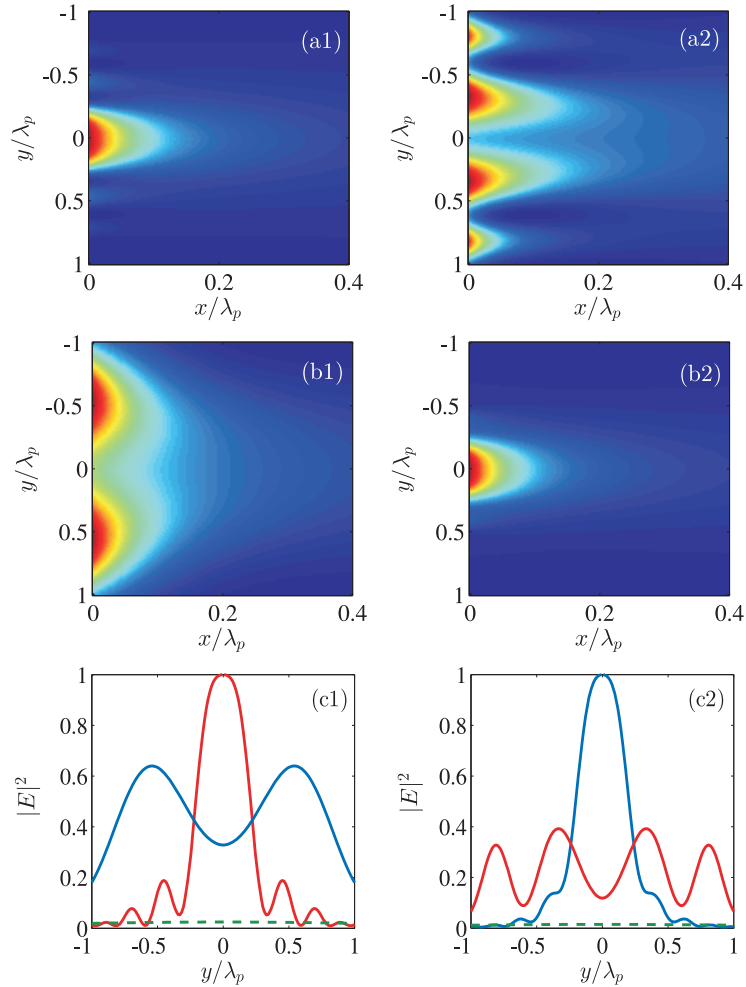


Fig. 4. Transmitted electric-field intensity distribution for a line dipole source $\mathbf{J} = \delta(x + l + x_s)\delta(y)\hat{y}$ positioned to the left of a HMM slab that has its left interface at $x = -l$ and right interface at $x = 0$. For $\omega = 0.41\omega_p \approx \omega_{\text{res}}^{\text{loc}}$, panel (a1) shows the intensity for local response, (b1) for nonlocal response, and (c1) the intensity along y with $x = 0$. Panels (a2), (b2), and (c2) are the analogous graphs for $\omega = 0.465\omega_p \approx \omega_{\text{res}}^{\text{nlloc}}$. In panels (c1) and (c2), the green dashed curves are for the case without the HMM slab, the red solid curves for the HMM with local response, and the blue solid curves for the HMM with nonlocal response. The HMM unit cell is as that in Fig. 1, $x_s = 10\text{nm}$ and $l = 36d$. The spatial coordinates in all figures are normalized by the free space wavelength at plasma frequency denoted as λ_p .

tions do exist. However, the transmission coefficients for the different wave components vary more smoothly as a function of \mathbf{k}_{\parallel} , thanks to the flat dispersion curve with the constant k_{\perp} . Accordingly, after propagation through the HMM from $x = -l$ to $x = 0$, an image is formed near $x = 0$, as seen in Fig. 4(a1). The size of the image is approximately $\lambda_p/2$, i.e., $0.2\lambda_0$ with λ_0 being the operating wavelength corresponding to $\omega_0 = 0.41\omega_p$, so that the size of the image is in the subwavelength scale. By contrast, in the nonlocal case the dispersion curve turns into an ellipse. This closed dispersion curve sets an upper wavevector cutoff for the evanescent waves, and the wave components below the cutoff experience different phase changes. Accordingly,

the quality of the image becomes worse, see Fig. 4(a2).

In Fig. 4(c1), we depict the electric-field intensity again at $\omega_{\text{res}}^{\text{loc}}$ as a function of y at the HMM boundary $x = 0$, and also for the case without the HMM slab. It is seen that the electric-field intensity is nearly vanishing in the absence of the HMM slab, since the evanescent components vanish after traveling a distance of l , which is of the order of one free-space wavelength. With the HMM slab in place, the electric-field intensity in the local case shows a subwavelength image that peaks at $y = 0$, with a full width at half maximum (FWHM) of only $0.42\lambda_p$. With nonlocal response, however, the electric-field intensity distribution for $\omega_{\text{res}}^{\text{loc}}$ becomes flatter, with a double rather than a single peak, with peak intensities at $y = \pm 0.55\lambda_p$.

Let us now turn to the other resonance frequency, namely $\omega = \omega_{\text{res}}^{\text{nlloc}}$ of Eq. (12). Figure 4(a2) and (b2) show the transmitted electric-field intensity for the local and nonlocal cases, respectively, at $\omega = \omega_{\text{res}}^{\text{nlloc}} = 0.465\omega_p$. At this frequency, the local dispersion curve is a hyperbola, while the nonlocal dispersion shows two flat lines. In the nonlocal case, we have $k_{\perp}l \approx 5\pi$, and this value of nearly an integer times π indicates that reflections are nearly zero. As a result, the hydrodynamic Drude model predicts a better focusing performance of the HMM slab at $\omega = 0.465\omega_p = \omega_{\text{res}}^{\text{nlloc}}$ than does the local-response theory, compare Fig. 4(a2) and (b2). In Fig. 4(c2), the electric-field intensity along y at $x = 0$ is shown. In the local case, the electric-field intensity shows several peaks with the strongest two at $y = \pm 0.33\lambda_p$. In the nonlocal case, the electric-field intensity is peaked at $y = 0$ with a subwavelength FWHM of only $0.4\lambda_p$.

6. Detecting nonlocal response by near-field measurement

Figure 4 indicates the possibility of detecting the nonlocal response experimentally by measuring the transmitted near-field distribution at the surface of a HMM superlens, which in our setup would be its right interface at $x = 0$. The images in Fig. 4(c1,c2) correspond to hypothetical measurements with infinitely small detectors. In experiments, the measured near-field signal will rather be an area-averaged electric-field intensity

$$I_{\text{av}} \propto \frac{1}{D} \int_D d^2\mathbf{r} |\mathbf{E}(\mathbf{r})|^2, \quad (13)$$

where D is the finite detection area of the detector. Let us now assume that we have a near-field detector with detection area in the yz -plane, with a square shape of size $40\text{ nm} \times 40\text{ nm}$, touching the HMM interface at $x = 0$. For the same light source interacting with the HMM slab as in Fig. 4, we depict in Fig. 5 the calculated I_{av} as a function of the y -coordinate of the center of the detector. It is seen that local and nonlocal response models give significantly different predictions for the measured signal, and thus the differences between the two models survive detection area averaging. The single peaks at $0.41\omega_p$ for local response and at $0.465\omega_p$ for nonlocal response are naturally broader than in Fig. 4(c1,c2), also due to the area averaging. Interestingly, as the frequency increases from $0.41\omega_p$ to $0.465\omega_p$, the distribution of I_{av} becomes broader in the LRA, but narrower in the hydrodynamic Drude model.

7. Conclusions

We investigated the effects of the hydrodynamic nonlocal response on hyperbolic metamaterials with periodicity in the subwavelength regime of the transverse optical wave, but much larger than the wavelength of the longitudinal hydrodynamic pressure waves. It is found that the nonlocal response corrects the effective permittivity tensor element $\epsilon_{\perp}^{\text{loc}}$ in the periodicity direction to the new form $\epsilon_{\perp}^{\text{nlloc}}$ of Eq. (10). Around the frequencies $\omega_{\text{res}}^{\text{loc}}$ and $\omega_{\text{res}}^{\text{nlloc}}$ corresponding to $\epsilon_{\perp}^{\text{loc}} \rightarrow \infty$ and $\epsilon_{\perp}^{\text{nlloc}} \rightarrow \infty$, respectively, $\epsilon_{\perp}^{\text{loc}}$ and $\epsilon_{\perp}^{\text{nlloc}}$ show noticeable differences, even leading to completely different dispersion curves with and without the nonlocal response.

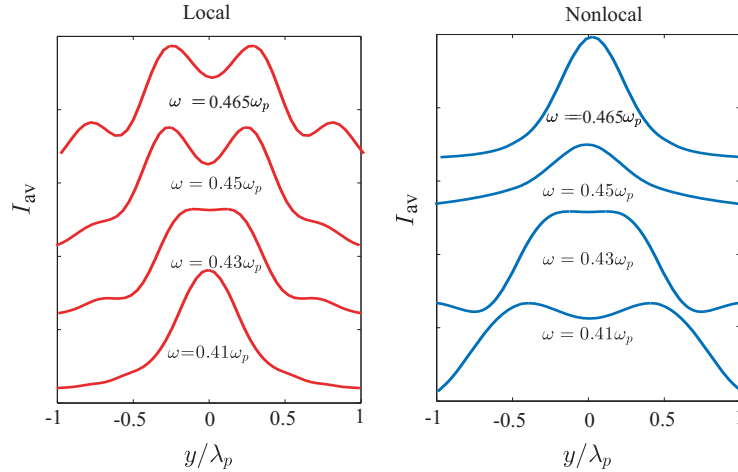


Fig. 5. Calculated detector-area-averaged near-field intensity I_{av} of the light emitted by the same source as in Fig. 4 and transmitted through the same HMM slab. The detector is square-shaped with size $40\text{nm} \times 40\text{nm}$, touching the HMM right interface at $x = 0$. It scans along the y -direction, and the y -coordinate on the horizontal axes in panels (a) for the LRA and (b) for the HDM corresponds to that of the center of the detector.

We find that nonlocal response blueshifts the resonance frequency of HMMs from $\omega_{\text{res}}^{\text{loc}}$ [Eq. (11)] to $\omega_{\text{res}}^{\text{nlc}}$ [Eq. (12)]. The relative blueshift has an interesting simple form independent of the thickness of the metal layers. Similar nonlocal blueshifts for single nanoplasmonic particles have been predicted before, and significant blueshifts have also been measured [27, 29]; how much of these can be attributed to hydrodynamic effects is a hot topic [27, 29, 35]. Similar discussions apply to nanowire dimers [36–38].

Furthermore, we predict that nonlocal response shows its mark in the performance of a finite HMM slab as a focusing lens: when increasing the operating frequency from $\omega_{\text{res}}^{\text{loc}}$ to $\omega_{\text{res}}^{\text{nlc}}$, for local response the near-field distribution of the transmitted light shows an image that gets out of focus, whereas the focus would improve instead according to the nonlocal-response theory. We propose to test the blueshift and these contrary predictions experimentally, as a clear and interesting test whether nonlocal response can be observed in hyperbolic metamaterials.

Acknowledgments

This work was financially supported by an H. C. Ørsted Fellowship (W.Y.) and the Center for Nanostructured Graphene is sponsored by the Danish National Research Foundation, Project DNRF58.